Supporting information for

Solar Thermal Activated Photocatalysis for Hydrogen Production and Aqueous Triethanolamine Polymerization

Jinghui Wang[a, †], Ziping Wang[a, d, †], Xia Wang[a], Peihe Li[a, *], Danhui Sun[a], Limei Duan[a], Jie Bai[c], Sarina Sarina[b], Huaiyong Zhu[b], Jinghai Liu[a, *]

[a]*Inner Mongolia Key Laboratory of Carbon Nanomaterials, Inner Mongolia Engineering Research Center of Lithium-Sulfur Battery Energy Storage, Nano Innovation Institute (NII), College of Chemistry and Materials Science, Inner Mongolia Minzu University, Tongliao 028000, People's Republic of China. Email: jhliu2008@sinano.ac.cn; phli2018@foxmail.com; Fax: 86-475-8313570; Tel: 86-475-8314342*

[b]*School of Chemistry, Physics and Mechanical Engineering, Queensland University of Technology, Brisbane, QLD, 4001, Australia*

[c]*Chemical Engineering College, Inner Mongolia University of Technology, Huhhot 010051, People' s Republic of China*

[d]*National & Local United Engineering Laboratory for Power Battery, Department of Chemistry, Northeast Normal University, Changchun 130024, People' s Republic of China*

† J.H.W.and Z.P.W. contribute equally to the work

Figure and Table list:

irradiation.

Fig. S23 NBO charges analysis for the calculated Pt_6-CN, H-Pt_6-CN and H_2-Pt_6-CN.

Fig. S24 (a) Schematic chemical structure of g-C_3N_4. (b) Surface electrostatic potential distribution of g-C_3N_4. (c) Surface electrostatic potential distribution of Pt cluster-carbon nitride (Pt_6-CN).

Fig. S25 The nuclear magnetic resonance (NMR) spectrum for TEOA polymerization product.

Fig. S26 Scheme for free radical polymerization of TEOA initiated by STAP hole-mediating radical reactions.

Fig. S27 The mass spectrum (part) of TEOA polymerization product.

Fig. S28 Infrared camera images of solution temperature change under irradiation.

Fig. S29 The particle size of (a) g-C_3N_4-CQ/Pt, (b) g-C_3N_4-H1/Pt, (c) g-C_3N_4-HG/Pt, (d) g-C_3N_4-OM/Pt, (e) g-C_3N_4-T/Pt.

Table S1. Atomic percentage and atomic ratio for TEOA polymerization production

Table S2. XPS atomic percentage analysis of Pt deposited g-C_3N_4 samples

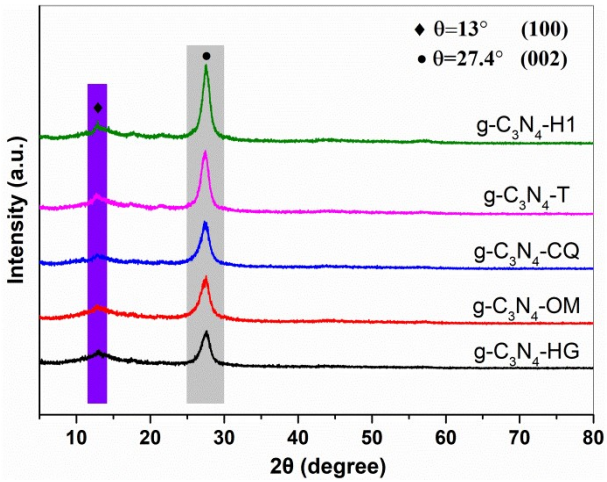

Fig. S1 XRD patterns of the g-C_3N_4 samples.

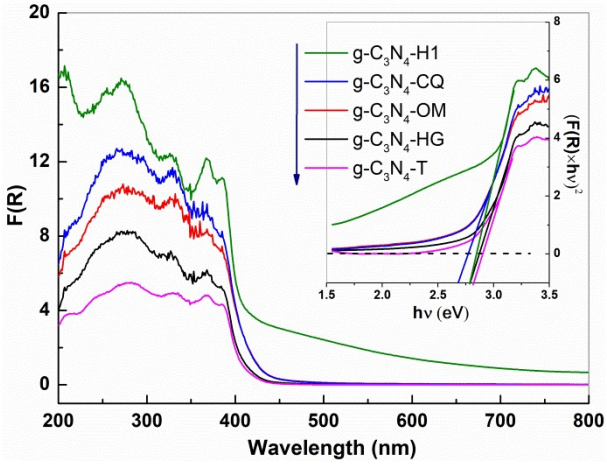

Fig. S2 UV-Vis DRS of the g-C_3N_4 samples. Insets, the Tauc plots.

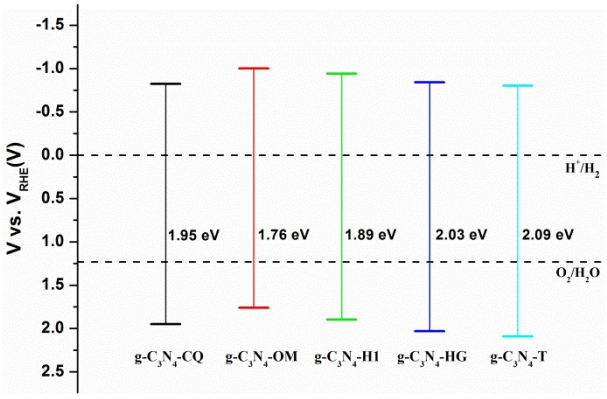

Fig. S3 The band-gap structure of the g-C_3N_4 samples.

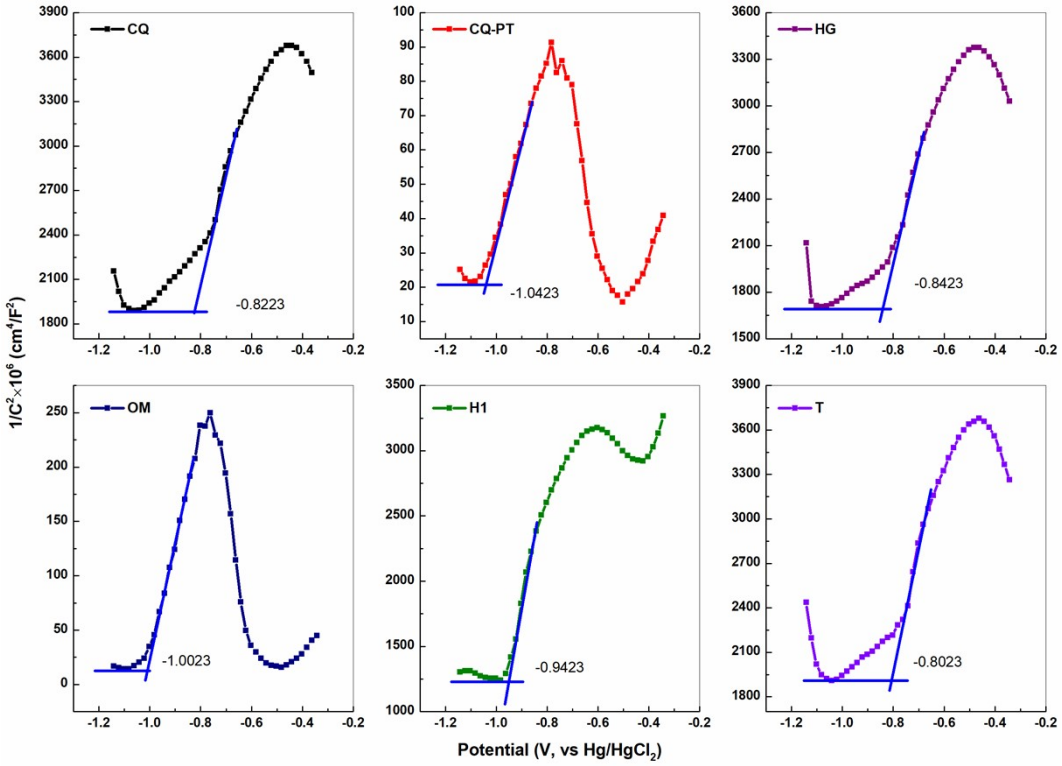

Fig. S4 Mott-Schottky plots for (a) g-C_3N_4-CQ, (b) g-C_3N_4-CQ/Pt, (c) g-C_3N_4-HG, (d) g-C_3N_4-OM, (e) g-C_3N_4-H1, (f) g-C_3N_4-T.

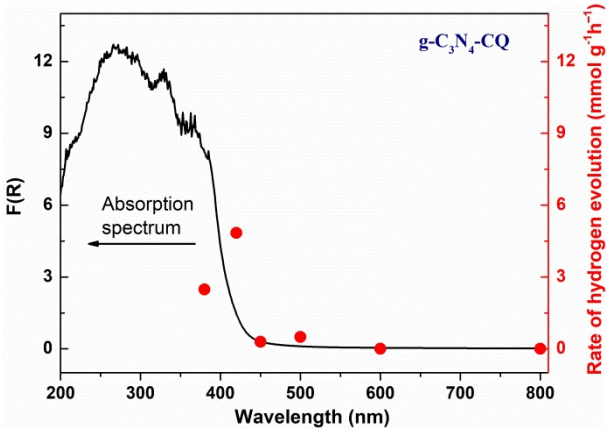

Fig. S5 The absorption of the g-C_3N_4-CQ with the rate of hydrogen evolution under the monochromatic light irradiation.

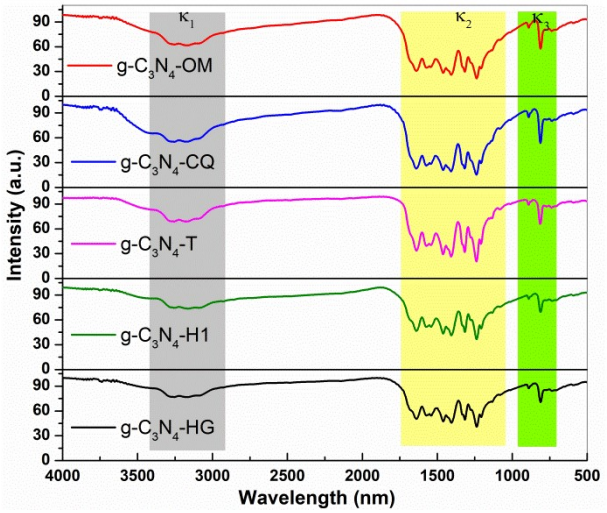

Fig. S6 FTIR of the g-C_3N_4 samples.

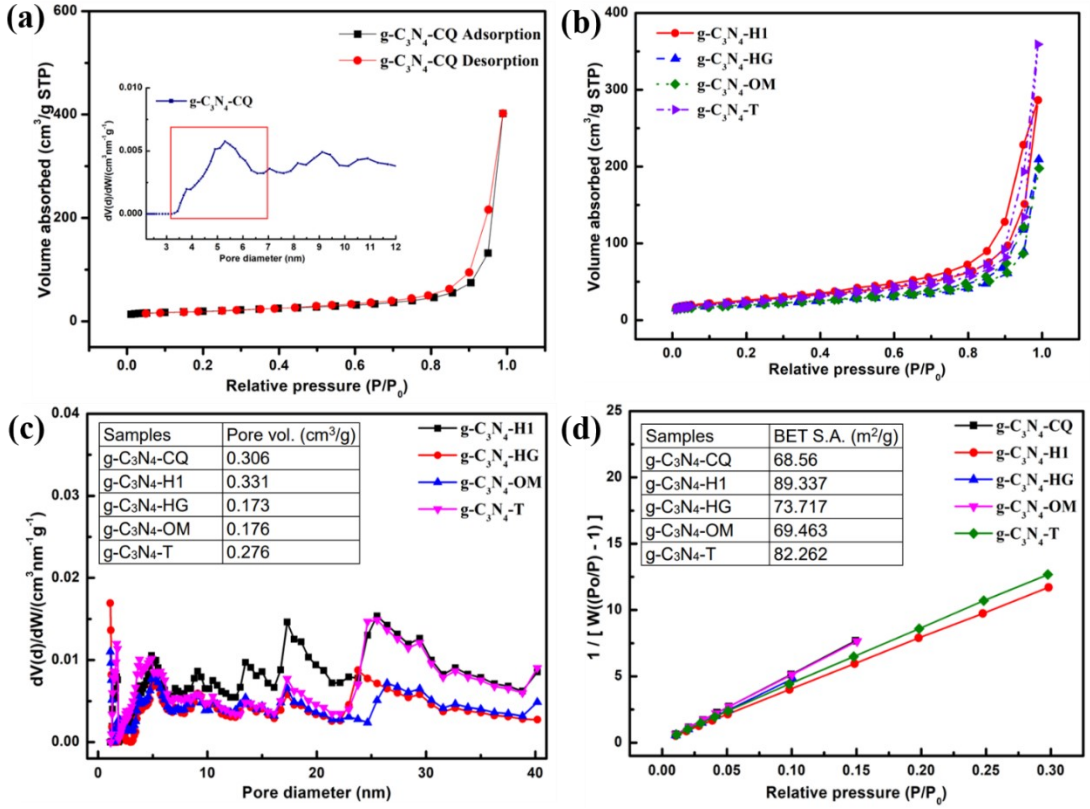

Fig. S7 (a-b) Nitrogen adsorption/desorption isotherms. (c) Pore size distribution analysis. (d) Specific surface area and BET plots.

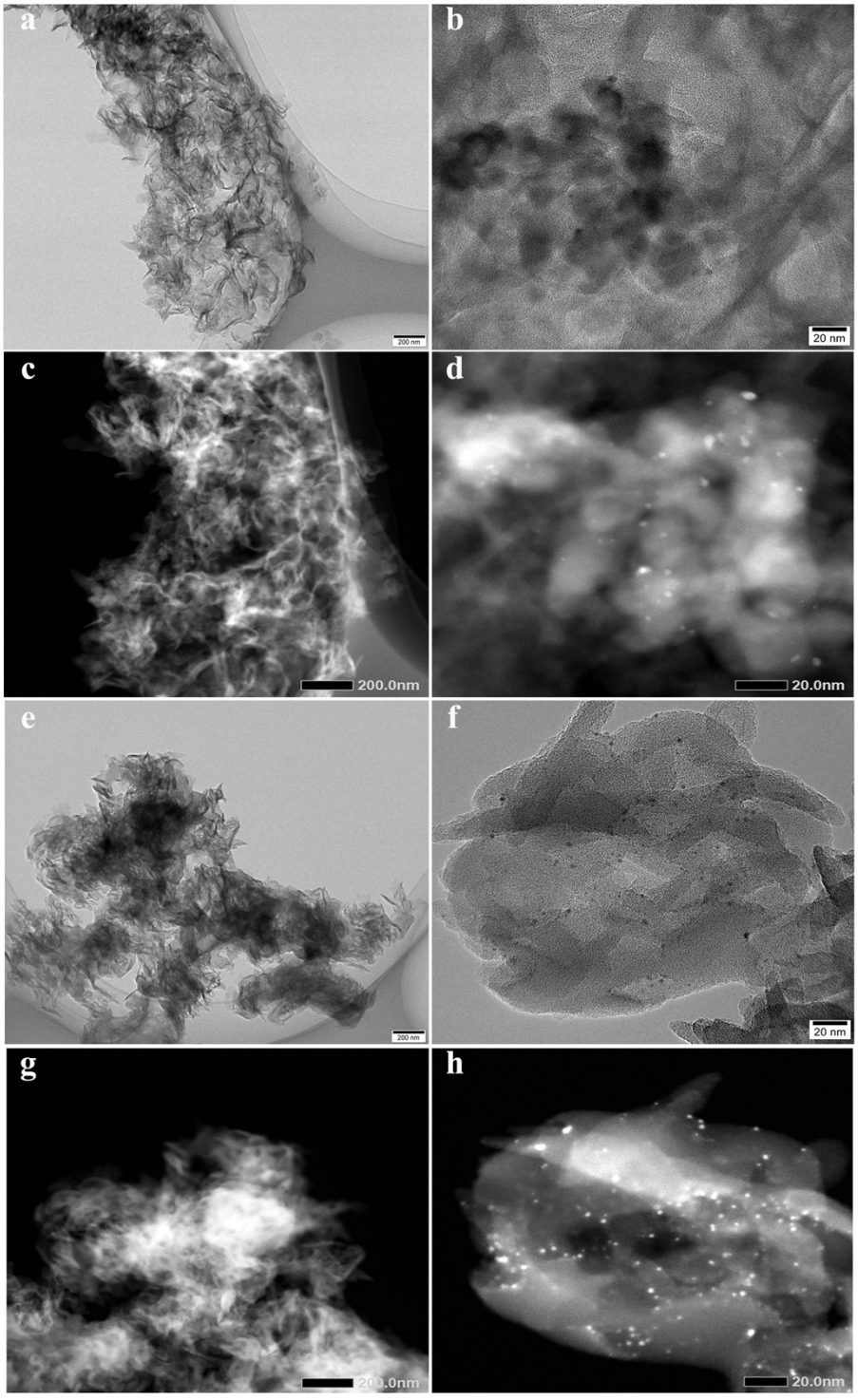

Fig. S8 TEM and corresponding HAAD-STEM images for g-C_3N_4-H1 (a) and (c), g-C_3N_4-H1/Pt (b) and (d), g-C_3N_4-HG (e) and (g), g-C_3N_4-HG/Pt (f) and (h).

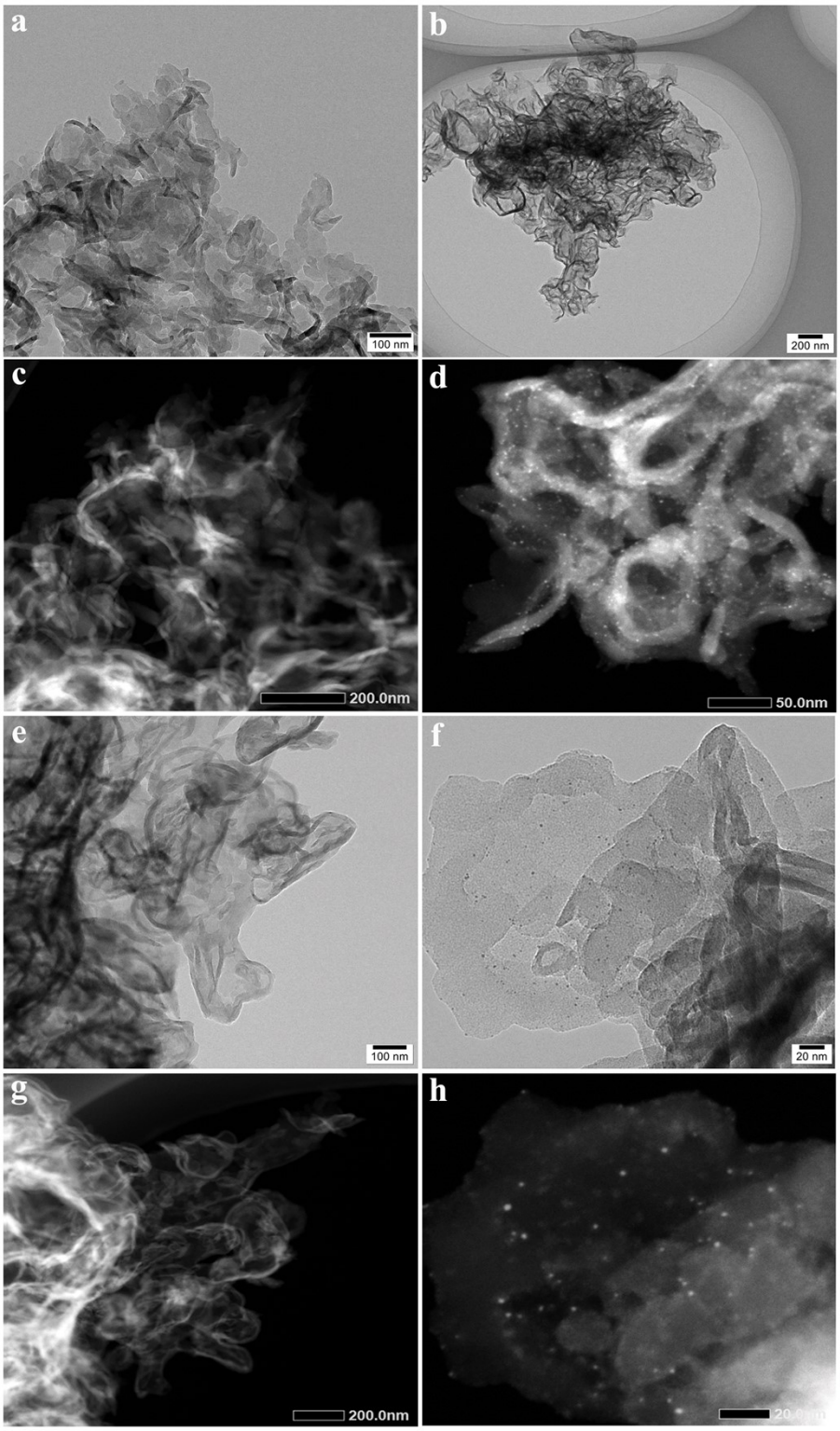

Fig. S9 TEM and corresponding HAAD-STEM images for g-C_3N_4-OM (a) and (c), g-C_3N_4-OM/Pt (b) and (d), g-C_3N_4-T (e) and (g), g-C_3N_4-T/Pt (f) and (h).

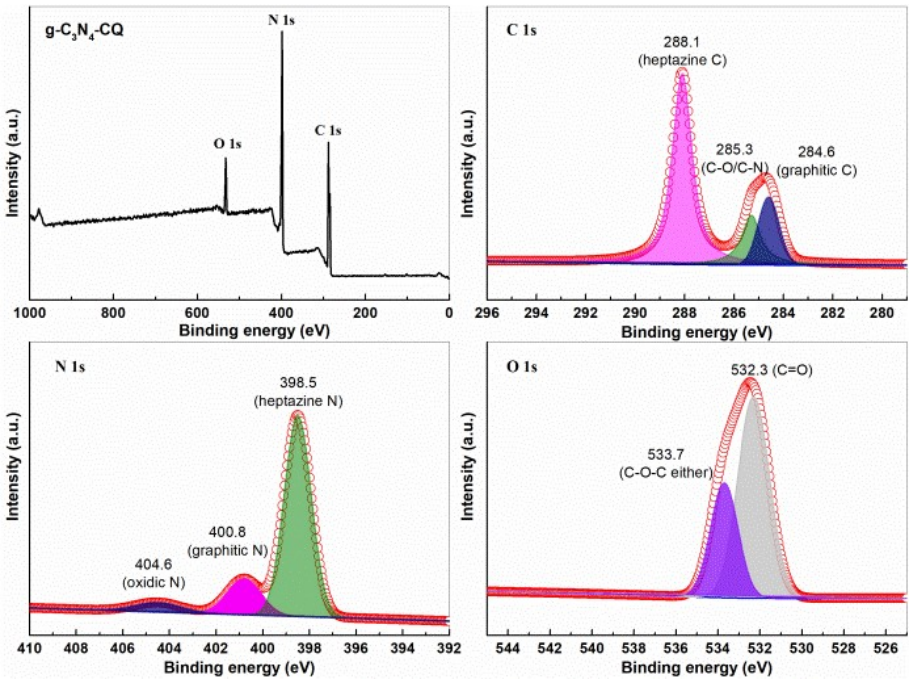

Fig. S10 XPS spectra of the g-C_3N_4-CQ. (a) XPS survey. High-resolution C 1s (b), N 1s (c) and O 1s (d).

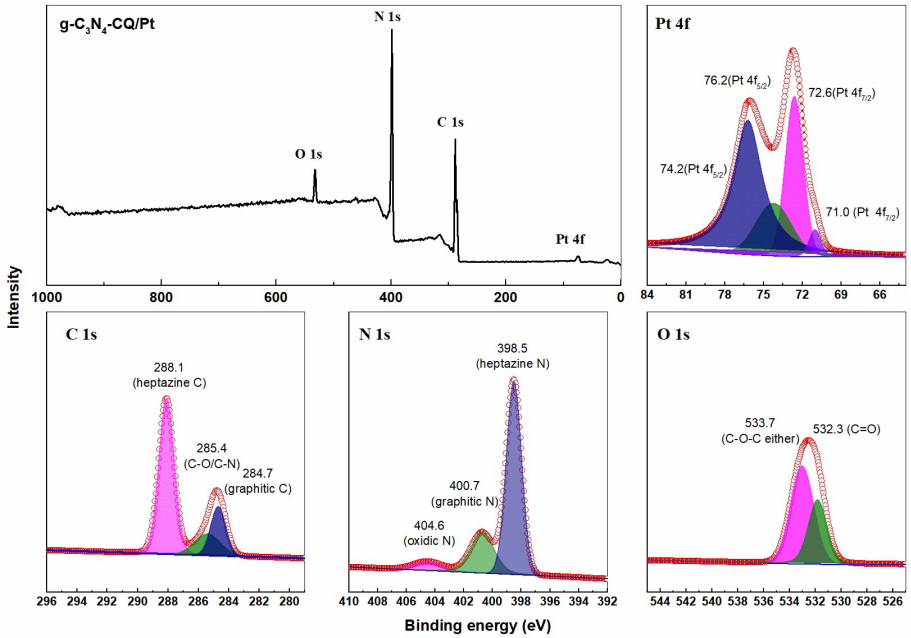

Fig. S11 XPS spectra of the g-C_3N_4-CQ/Pt. (a) XPS survey. High-resolution Pt 4f (b), C 1s (c), N 1s (d) and O 1s (e).

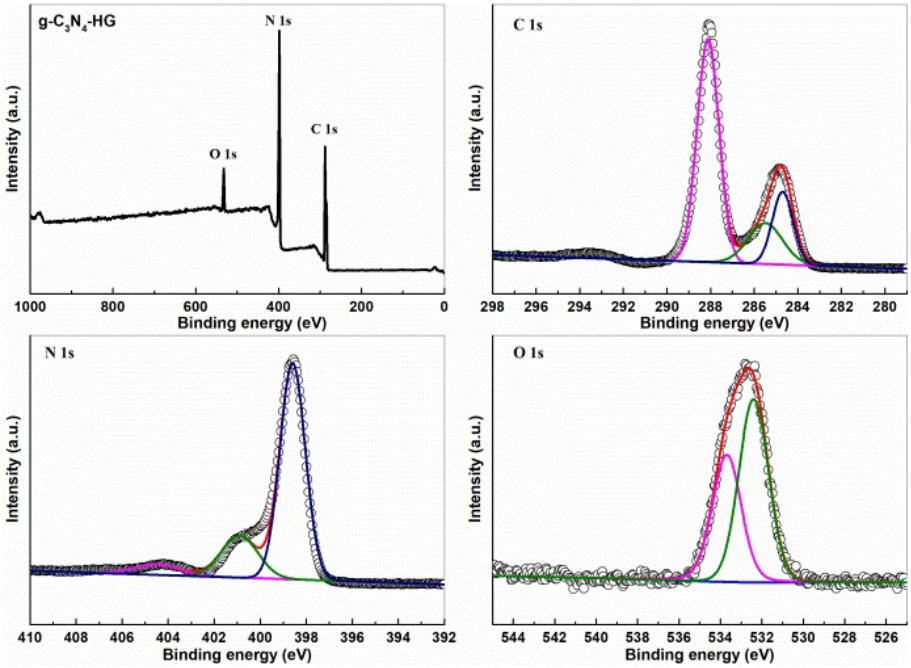

Fig. S12 XPS spectra of the g-C_3N_4-HG. (a) XPS survey. High-resolution C 1s (b), N 1s (c) and O 1s (d).

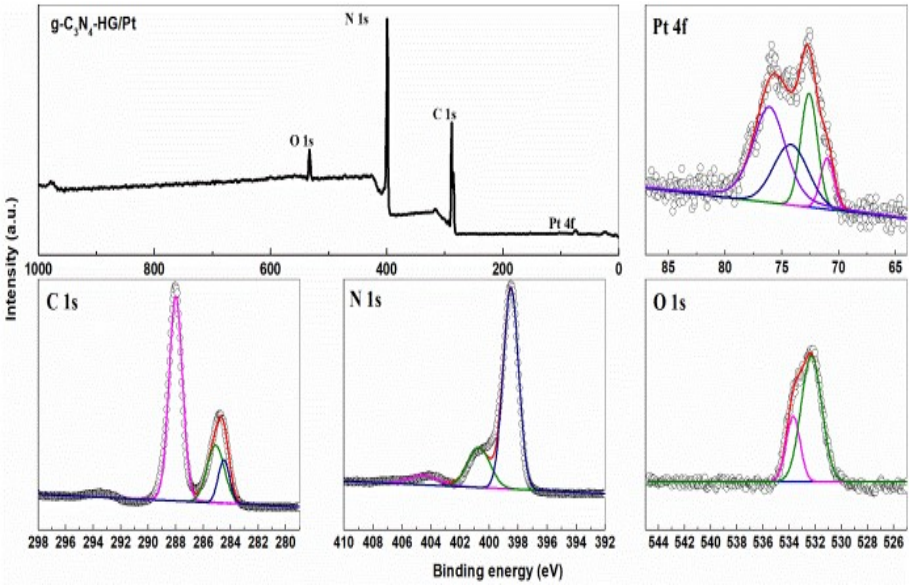

Fig. S13 XPS spectra of the g-C_3N_4-HG/Pt. (a) XPS survey. High-resolution Pt 4f (b), C 1s (c), N 1s (d) and O 1s (e).

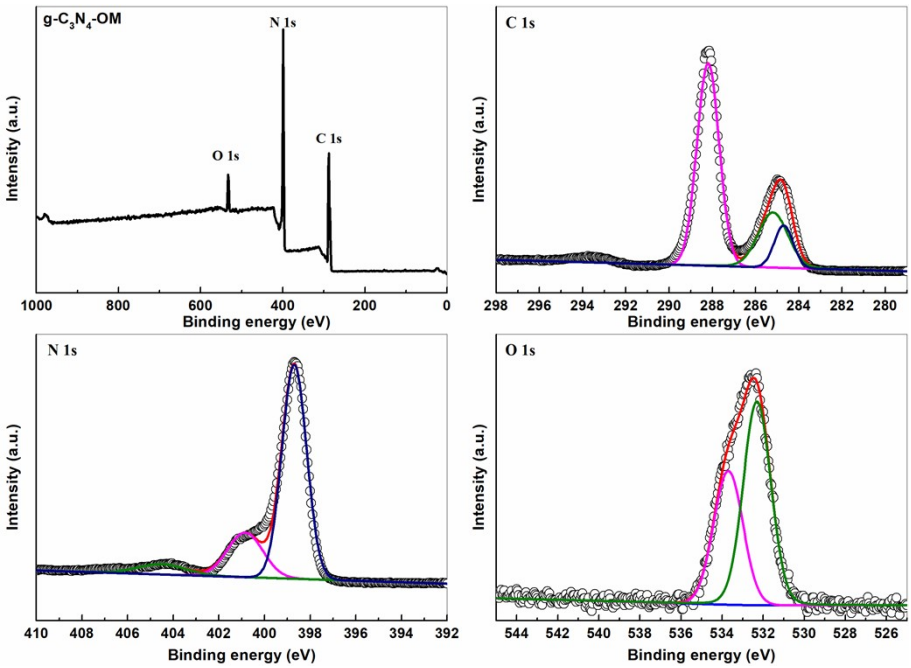

Fig. S14 XPS spectra of the g-C_3N_4-OM. (a) XPS survey. High-resolution C 1s (b), N 1s (c) and O 1s (d).

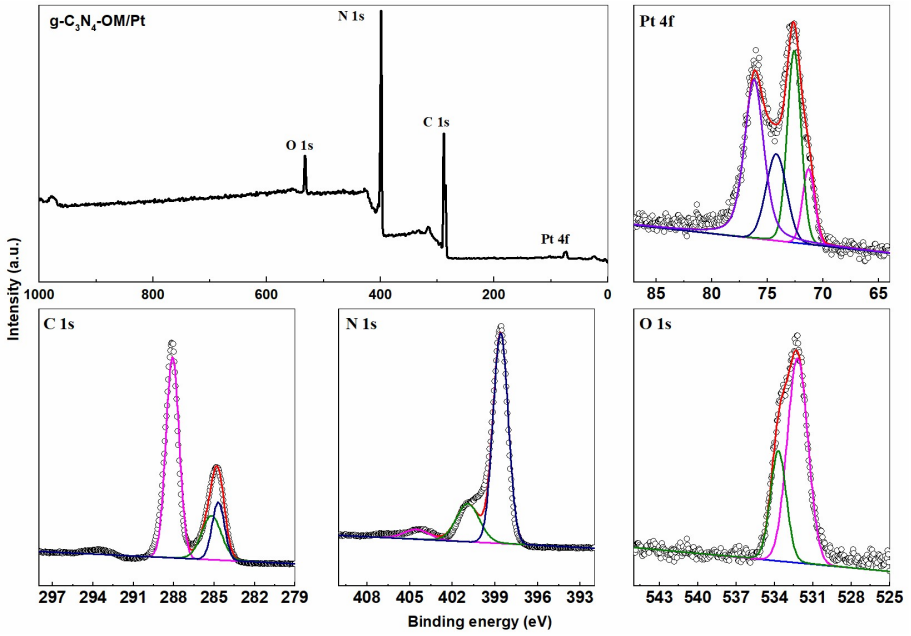

Fig. S15 XPS spectra of the g-C_3N_4-OM/Pt. (a) XPS survey. High-resolution Pt 4f (b), C 1s (c), N 1s (d) and O 1s (e).

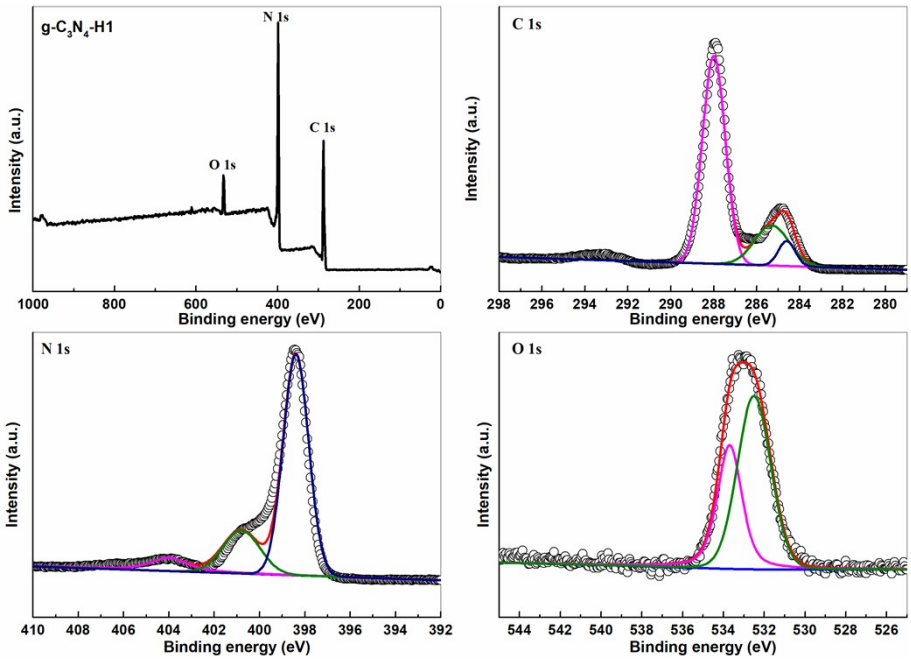

Fig. S16 XPS spectra of the g-C_3N_4-H1. (a) XPS survey. High-resolution C 1s (b), N 1s (c) and O 1s (d).

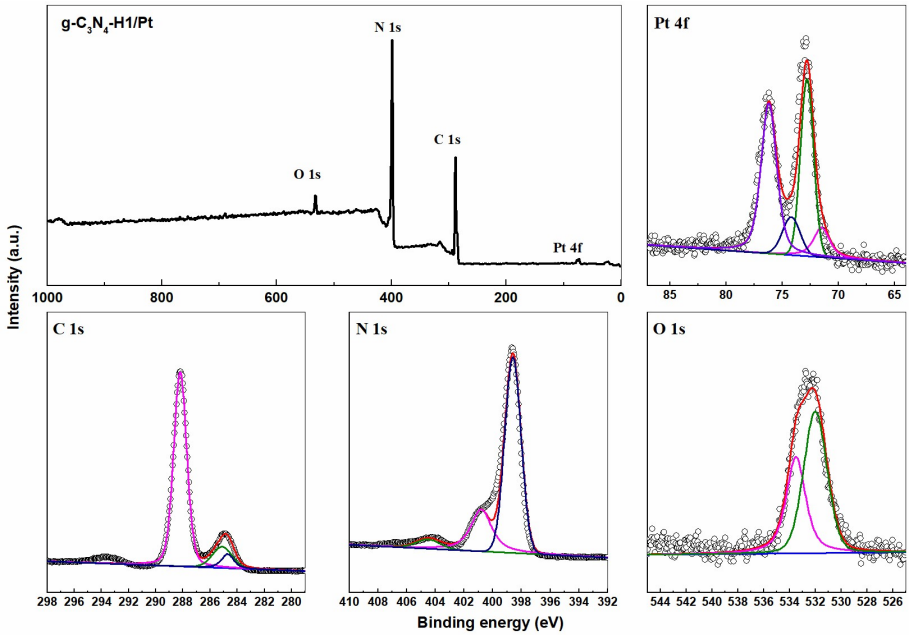

Fig. S17 XPS spectra of the g-C_3N_4-H1/Pt. (a) XPS survey. High-resolution Pt 4f (b), C 1s (c), N 1s (d) and O 1s (e).

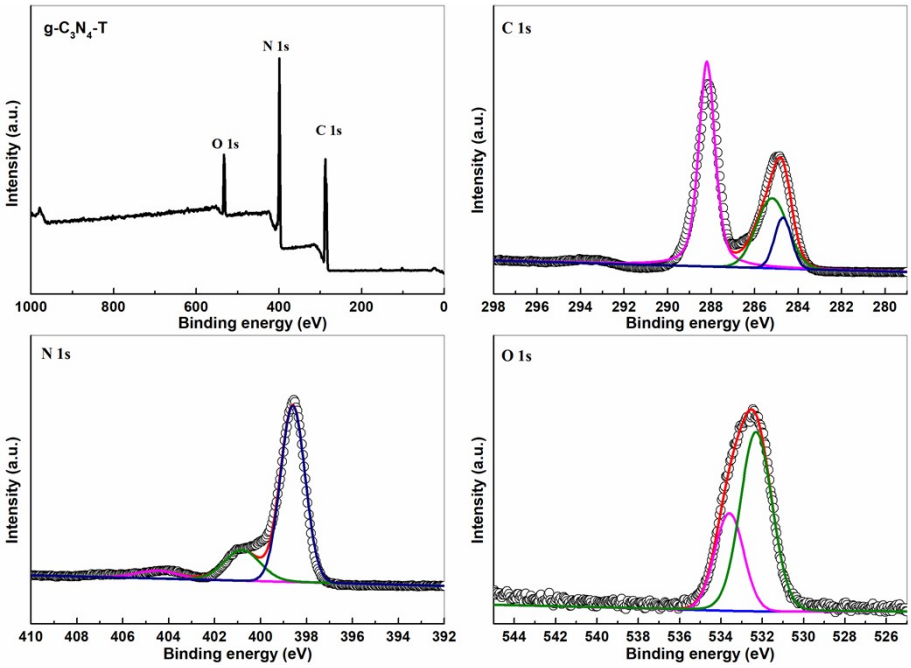

Fig. S18 XPS spectra of the g-C_3N_4-T. (a) XPS survey. High-resolution C 1s (b), N 1s (c) and O 1s (d).

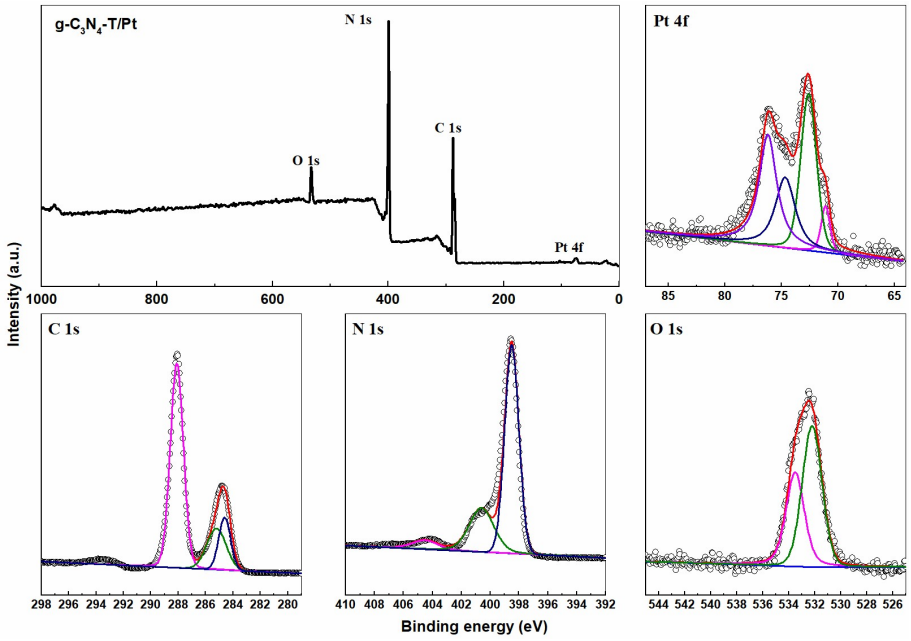

Fig. S19 XPS spectra of the g-C_3N_4-T/Pt. (a) XPS survey. High-resolution Pt 4f (b), C 1s (c), N 1s (d) and O 1s (e).

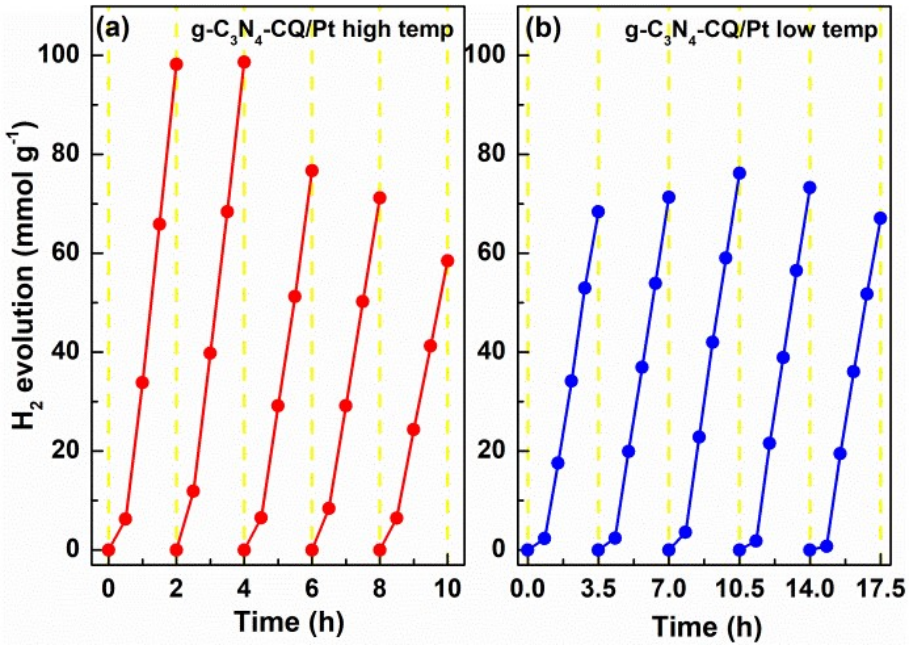

Fig. S20 Successive test runs for the HER on g-C_3N_4-CQ/Pt under visible light irradiation.

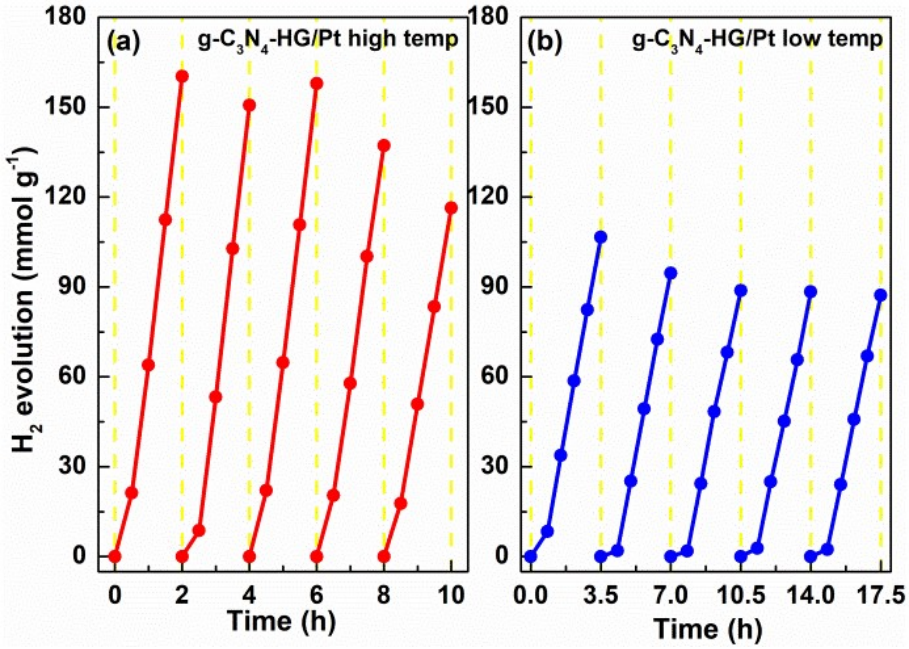

Fig. S21 Successive test runs for the HER on g-C_3N_4-HG/Pt under visible light irradiation.

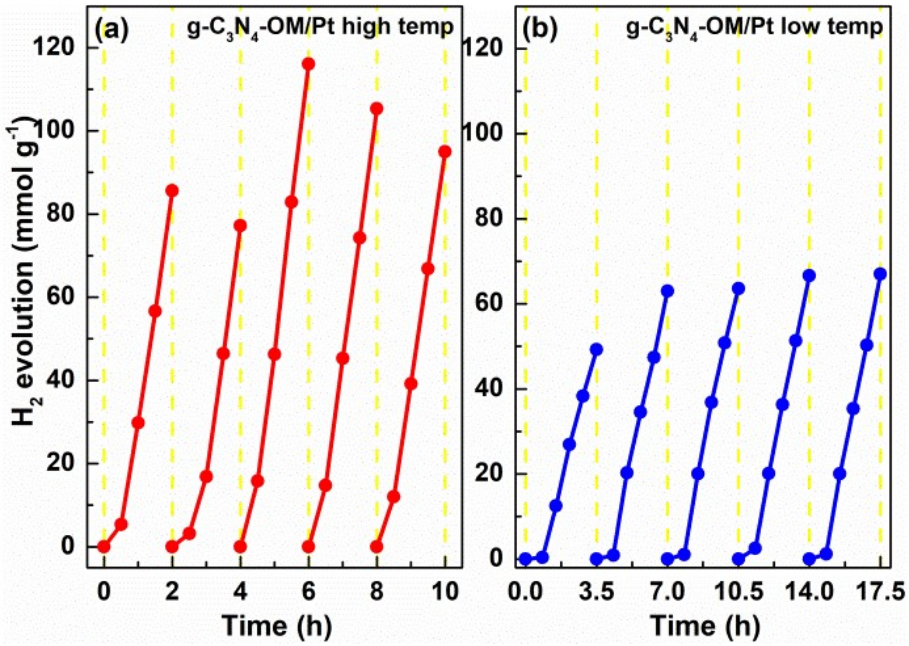

Fig. S22 Successive test runs for the HER on g-C_3N_4-OM /Pt under visible light irradiation.

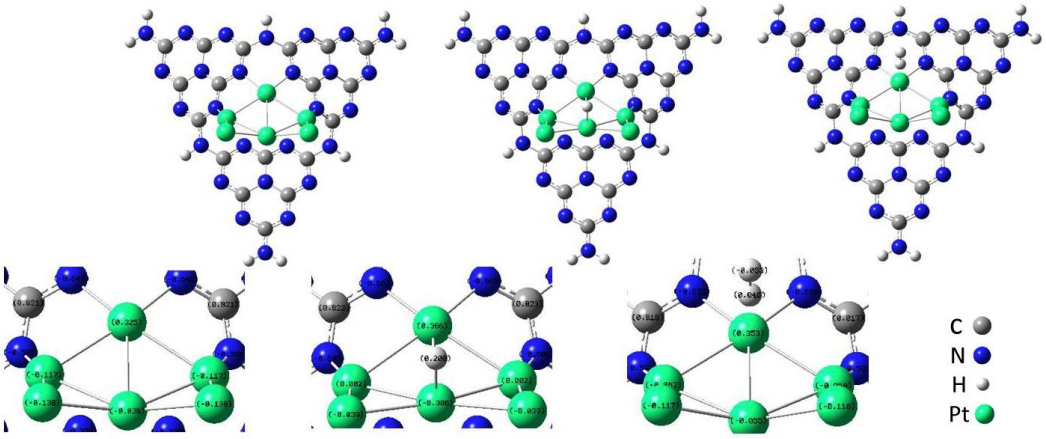

Pt_6	[core]6S(0.81)5d(9.05)6p(0.49)
Pt_6-H	[core]6S(0.40)5d(4.47)6p(0.37)
Pt_6-H_2	[core]6S(0.82)5d(9.01)6p(0.49)

18	57.887 kcal/mol
25	57.853 kcal/mol
36	57.801 kcal/mol

Fig. S23 NBO charges analysis for the calculated Pt_6-CN, H-Pt_6-CN and H_2-Pt_6-CN.

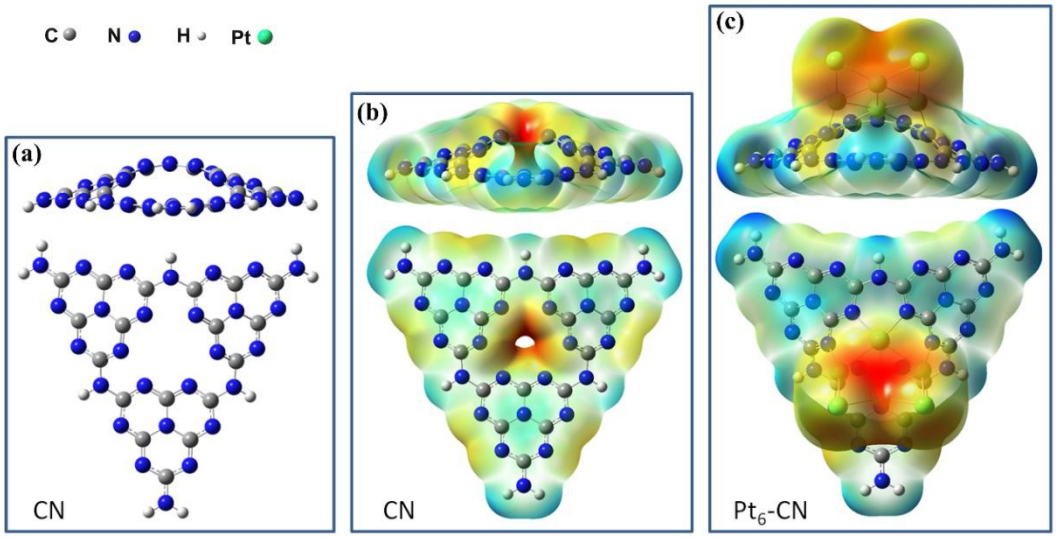

Fig. S24 (a) Schematic chemical structure of g-C_3N_4. (b) Surface electrostatic potential distribution of g-C_3N_4. (c) Surface electrostatic potential distribution of Pt cluster-carbon nitride (Pt_6-CN). Upper, side view. Below, vertical view

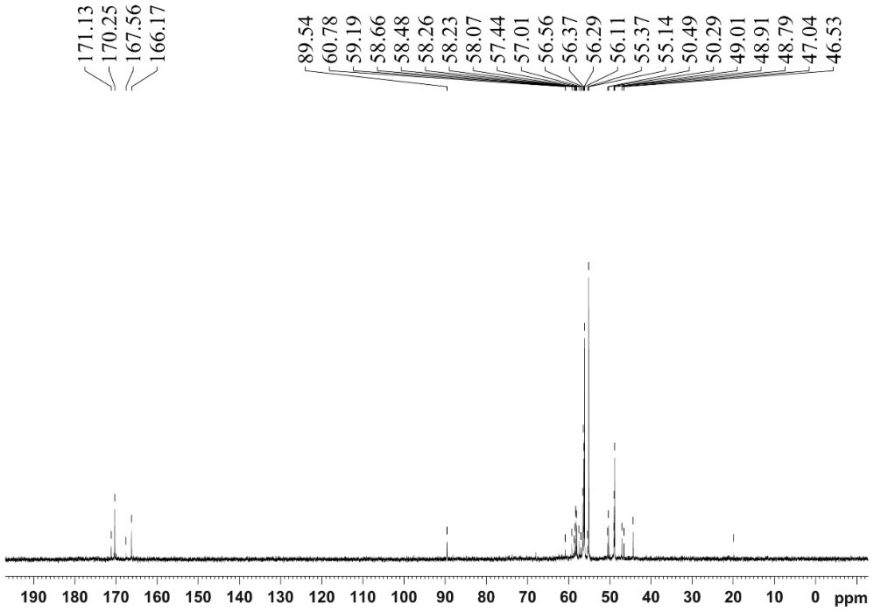

Fig. S25 The nuclear magnetic resonance (NMR) spectrum for TEOA polymerization product.

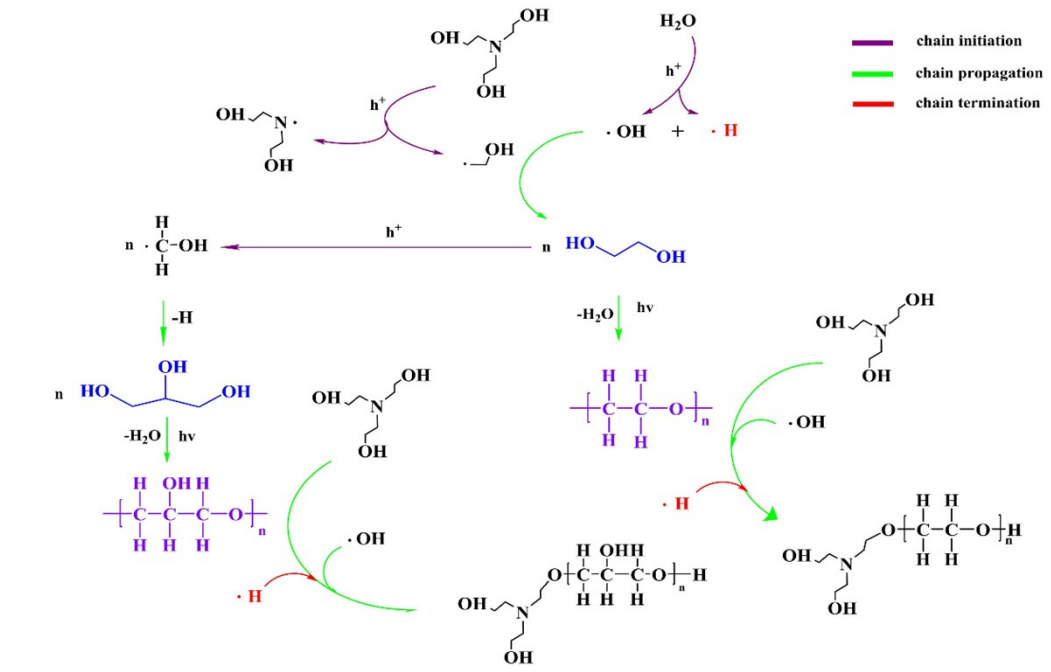

Fig. S26 Scheme for free radical polymerization of TEOA initiated by STAP hole-mediating radical reactions.

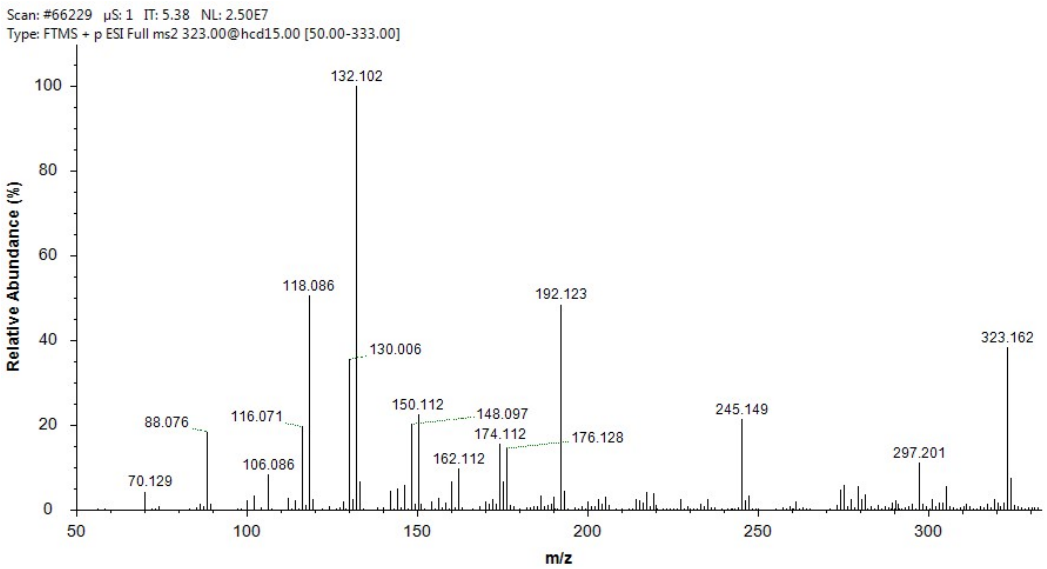

Fig. S27 The mass spectrum (part) of TEOA polymerization product.

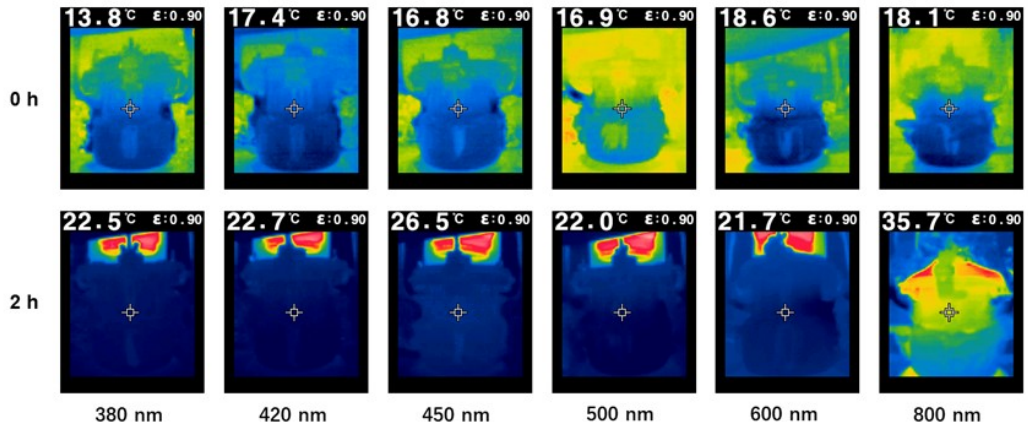
0 h
13.8℃ ε:0.90
17.4℃ ε:0.90
16.8℃ ε:0.90
16.9℃ ε:0.90
18.6℃ ε:0.90
18.1℃ ε:0.90
2 h
22.5℃ ε:0.90
22.7℃ ε:0.90
26.5℃ ε:0.90
22.0℃ ε:0.90
21.7℃ ε:0.90
35.7℃ ε:0.90
380 nm
420 nm
450 nm
500 nm
600 nm
800 nm

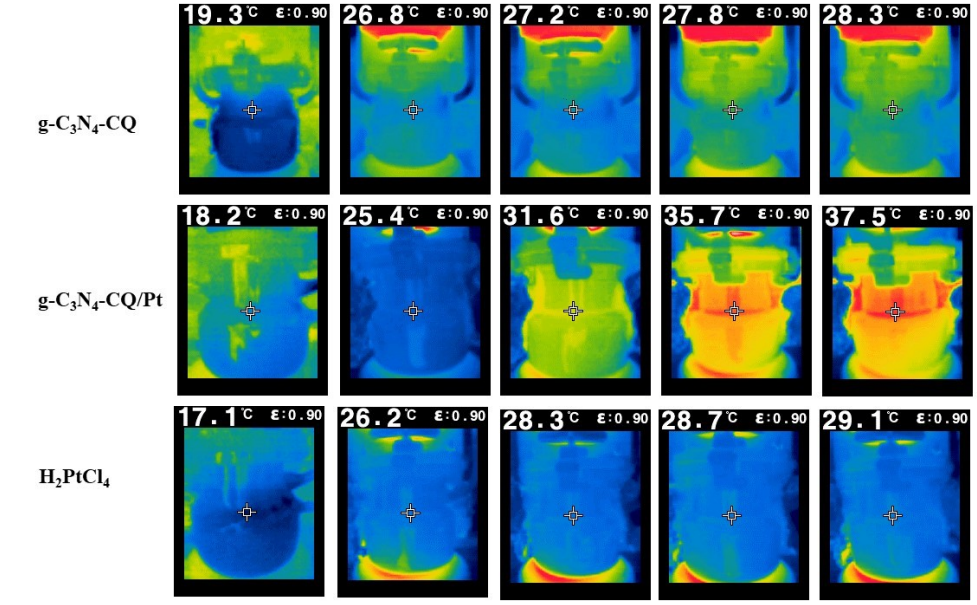
g-C3N4-CQ
19.3℃ ε:0.90
26.8℃ ε:0.90
27.2℃ ε:0.90
27.8℃ ε:0.90
28.3℃ ε:0.90
g-C3N4-CQ/Pt
18.2℃ ε:0.90
25.4℃ ε:0.90
31.6℃ ε:0.90
35.7℃ ε:0.90
37.5℃ ε:0.90
H2PtCl4
17.1℃ ε:0.90
26.2℃ ε:0.90
28.3℃ ε:0.90
28.7℃ ε:0.90
29.1℃ ε:0.90

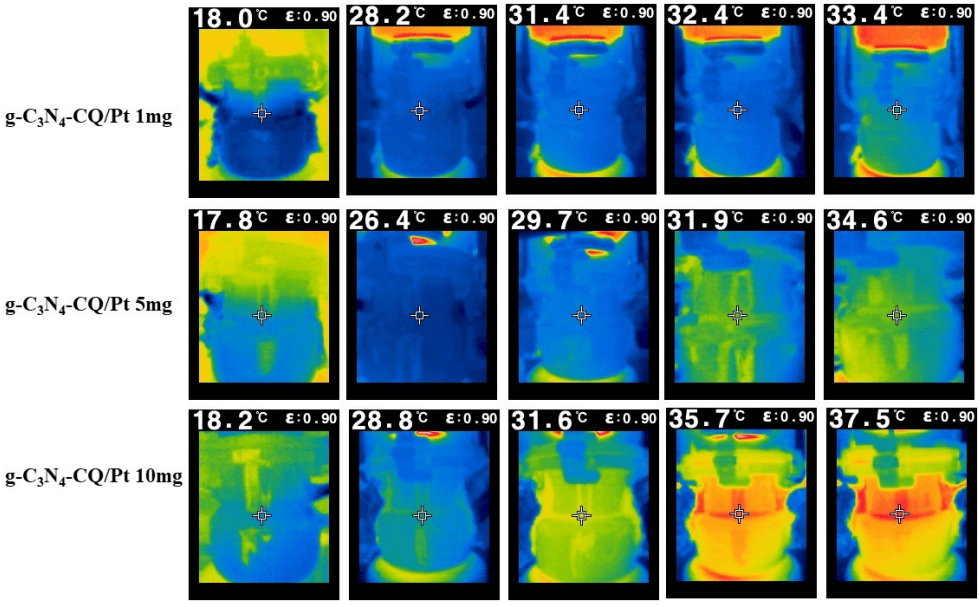
g-C3N4-CQ/Pt 1mg
18.0℃ ε:0.90
28.2℃ ε:0.90
31.4℃ ε:0.90
32.4℃ ε:0.90
33.4℃ ε:0.90
g-C3N4-CQ/Pt 5mg
17.8℃ ε:0.90
26.4℃ ε:0.90
29.7℃ ε:0.90
31.9℃ ε:0.90
34.6℃ ε:0.90
g-C3N4-CQ/Pt 10mg
18.2℃ ε:0.90
28.8℃ ε:0.90
31.6℃ ε:0.90
35.7℃ ε:0.90
37.5℃ ε:0.90

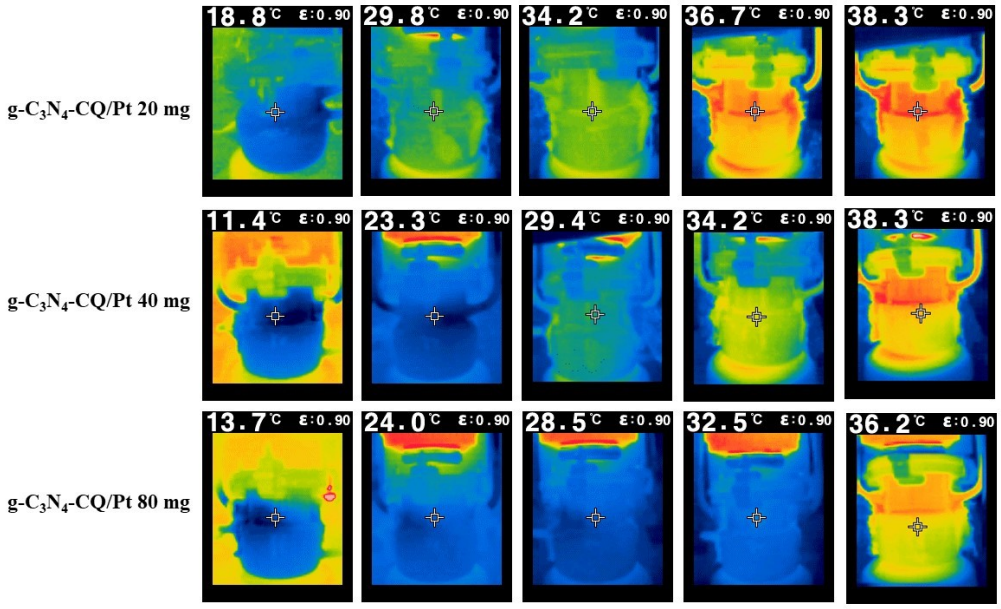

Fig. S28 Infrared camera images of solution temperature change under irradiation.

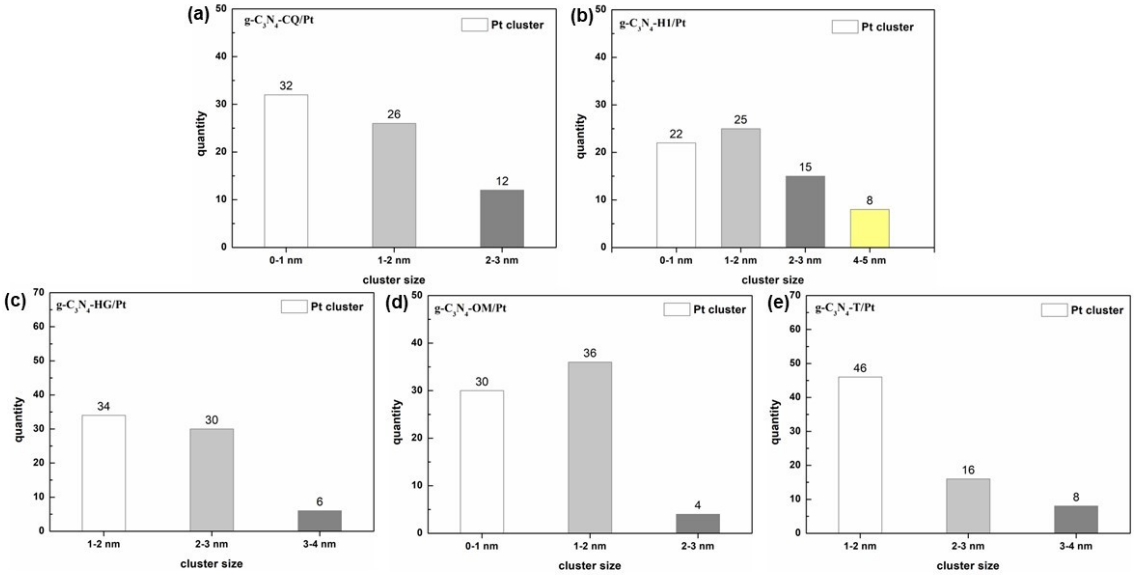

Fig. S29 The particle size of (a) g-C_3N_4-CQ/Pt, (b) g-C_3N_4-H1/Pt, (c) g-C_3N_4-HG/Pt, (d) g-C_3N_4-OM/Pt, (e) g-C_3N_4-T/Pt.

Table S1. Atomic percentage and atomic ratio for TEOA polymerization production

Weight (mg)	N (%)	C (%)	H (%)	S (%)	C/N ratio	C/H ratio	Atomic ratio
0.9030	3.79	42.77	6.058	0.781	11.2718	7.0607	$C_{13.2}NH_{22.4}O_{10.8}$

Table S2. XPS atomic percentage analysis of Pt deposited g-C_3N_4 samples

	C 1s (Atomic %)	N 1s (Atomic %)	O 1s (Atomic %)	Pt 4f (Atomic %)	Pt 4f (wt%)
g-C_3N_4-CQ	52.45	41.00	6.55		
g-C_3N_4-CQ/Pt	50.67	44.35	4.75	0.23	0.0012
g-C_3N_4-HG	51.40	42.84	5.76		
g-C_3N_4-HG/Pt	51.22	44.28	4.34	0.16	0.0008
g-C_3N_4-OM	51.08	43.94	4.99		
g-C_3N_4-OM/Pt	51.13	43.53	5.06	0.28	0.0014
g-C_3N_4-H1	47.94	46.75	5.31		

g-C_3N_4-H1/Pt	45.53	51.01	3.27	0.18	0.0009
g-C_3N_4-T	54.77	37.91	7.33		
g-C_3N_4-T/Pt	50.46	44.82	4.52	0.20	0.0010